



OPEN ACCESS

EDITED BY

Zhen Ma,
Fudan University, China

REVIEWED BY

Xiaocui Wei,
Hainan University, China
Tian-Sheng Zhao,
Ningxia University, China
Houda Jouini,
Tunis University, Tunisia

*CORRESPONDENCE

Mduduzi N. Cele,
✉ mduduzi.Cele@nwu.ac.za

RECEIVED 17 January 2025

ACCEPTED 06 February 2025

PUBLISHED 25 February 2025

CITATION

Maseko P, Cele MN and Mdleleni MM (2025)
Olefin selectivity of K-Mn promoters on CoFe-
ZSM-5 based catalyst in CO₂ hydrogenation.
Front. Chem. 13:1562436.
doi: 10.3389/fchem.2025.1562436

COPYRIGHT

© 2025 Maseko, Cele and Mdleleni. This is an open-access article distributed under the terms of the [Creative Commons Attribution License \(CC BY\)](https://creativecommons.org/licenses/by/4.0/). The use, distribution or reproduction in other forums is permitted, provided the original author(s) and the copyright owner(s) are credited and that the original publication in this journal is cited, in accordance with accepted academic practice. No use, distribution or reproduction is permitted which does not comply with these terms.

Olefin selectivity of K-Mn promoters on CoFe-ZSM-5 based catalyst in CO₂ hydrogenation

Paula Maseko¹, Mduduzi N. Cele^{1*} and Masikana M. Mdleleni²

¹Department of Chemistry, North-West University, Mahikeng, South Africa, ²South African Institute for Advanced Materials Chemistry, University of Western Cape, Cape Town, South Africa

The conversion of carbon dioxide (CO₂), a major greenhouse gas, into light olefins is crucial for mitigating environmental impacts and utilizing non-petroleum-based feedstocks. Thermo-catalytic CO₂ transformation into valuable chemicals offers a promising solution to this challenge. This study investigates the effect of potassium (K) and manganese (Mn) promoters on CO₂ conversion and C₂H₄ selectivity over CoFe-ZSM-5 zeolites. Structural characterization via FTIR, pyridine-FTIR, and PXRD confirmed the successful incorporation of K and Mn into CoFe-ZSM-5 at 80°C without significant structural changes to the zeolite framework. BET analysis revealed that metal incorporation did not substantially alter the surface area, while SEM and TEM analyses confirmed the preservation of ZSM-5 spherical morphology. Fixed-bed reactor experiments conducted at 350°C and 20 bar demonstrated that K and Mn synergistically enhanced CO₂ conversion efficiency and selectivity toward C₂H₄. The K-Mn/4Fe4Co-ZSM-5 catalyst (modified with 4% Co and 4% Fe) exhibited the highest performance, achieving 97% olefin selectivity. Furthermore, Mn and K promoters reduce the CO selectivity on the Co-Fe-ZSM-5 catalyst. These findings underscore the critical role of K and Mn in facilitating efficient CO₂ activation and directing the reaction pathway toward valuable olefin products.

KEYWORDS

ZSM-5, carbon dioxide hydrogenation, ion exchange, promoters, selectivity, conversion

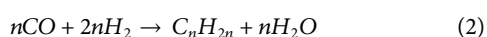
1 Introduction

The extensive use of fossil fuels has led to significant carbon dioxide (CO₂) emissions, contributing to pressing environmental issues such as global warming and ocean acidification (Abanades et al., 2017). South Africa, facing electricity shortages due to the depletion of coal reserves (Errero J.L. 2023), illustrates the urgent need for alternative solutions. CO₂ is a greenhouse gas and an abundant and cost-effective carbon source. Addressing the environmental impacts of CO₂ emissions involves capturing (Sun et al., 2023; Zhou et al., 2024), utilizing (Luo et al., 2023), and converting CO₂ (Ou et al., 2022; Tang et al., 2022; Luo et al., 2023). An effective strategy for mitigating CO₂ emissions involves chemically transforming CO₂ and green hydrogen into valuable products through thermo-, photo-, and electro-catalysis. This approach not only reduces CO₂ emissions but also provides essential feed-stock for various industries (Saeidi et al., 2014; Díez-Ramírez et al., 2017; Edelmánová et al., 2018; Tang et al., 2022; Gao et al., 2023). However, the hydrogenation of CO₂ to olefins presents challenges, including low selectivity, catalyst deactivation, and difficulties in controlling C-O bond activation and C-C bond formation (Weber et al., 2021; Jiang et al., 2023). To overcome these challenges, researchers are developing high-performance catalysts, particularly iron-based ones, by adjusting their

morphology, composition, and synthesis methods (Cele, 2014; Liu et al., 2022). Advances include exploring the effects of promoters, supports, and bifunctional catalysts to enhance olefin yields and improve catalyst stability (Weber et al., 2021). Despite progress, managing C-O activation and C-C coupling in long-chain hydrocarbon production remains a significant hurdle (Wei et al., 2021).

Recent studies have focused on bifunctional catalysts for CO₂ hydrogenation to olefins and aromatics, with promising results from Fe-based catalysts enhanced by elements like K, Mn, and Zn. Li et al. (2023) reported that FeMnKH-ZSM-5 achieved 70% selectivity for C₅-C₁₁ hydrocarbons and 17% for C₂-C₄ olefins at 320°C. García-Hurtado et al. (2020) found that the structure and size of zeolites influenced product selectivity, with MFI zeolites maximizing aromatic production and nanosized zeolites increasing light olefin selectivity. Liang et al. (2022) demonstrated that K-Zn-Fe/ZSM-5 catalysts achieved 45.2% aromatics selectivity with 42.6% CO₂ conversion. Xu et al. (2020) reviewed the synergistic effects of Mn and Na additives on Fe catalysts, which improved olefin selectivity and space-time yields. These findings highlight the critical role of catalyst composition, zeolite structure, and promoter interactions in optimizing CO₂ hydrogenation to produce valuable chemicals. Additionally, significant advancements have been made in the thermo-catalytic conversion of CO₂ into light olefins, methanol, ethanol, and aromatics (Sathawong et al., 2015; Li et al., 2017; Liu et al., 2021; Ojelade and Zaman, 2021; Wang and Zhang, 2023).

The synthesis of light olefins from CO₂ has gained considerable attention due to their importance as building blocks in the chemical industry (Li et al., 2017; Ronda-Lloret et al., 2019; Ojelade and Zaman, 2021; Muñoz and Weidema, 2024). Although traditional methods for olefin production, such as steam cracking and the methanol-to-olefins process, are well established (Al-Shafei et al., 2023; Wen et al., 2023; Muñoz and Weidema, 2024). Recent developments in multifunctional catalysts combining metal oxide nanoparticles with zeolites offer a promising pathway for CO₂ hydrogenation, albeit with challenges like co-product selectivity and insufficient olefin yields (Jiang et al., 2023; Wang and Zhang, 2023). The CO₂ Fischer-Tropsch (CO₂-FT) synthesis presents a promising route for converting CO₂ into light olefins with a higher single-pass yield (Raje et al., 1997; Visconti et al., 2016). This process involves converting CO₂ into olefins via the reverse water gas shift reaction (RWGS Equation 1) and the Fischer-Tropsch synthesis (FTS Equation 2):



Iron-based catalysts are preferred for CO₂-Fischer-Tropsch (FT) synthesis due to their high activity in both the reverse water-gas shift (RWGS) and FT reactions (Guo et al., 2022; Fedorov et al., 2023; Yang et al., 2023). However, using iron alone does not always lead to a high selectivity for light olefins; modification of the catalyst's chemical composition and structure is required. Typically, iron catalysts for CO₂ hydrogenation to light olefins are supported by oxides or carbon materials (Chen et al., 2023; Weber et al., 2023), with promoters often added to improve the yield of desired hydrocarbons by optimizing product distribution (Jiang et al., 2021; Chen et al., 2023; Weber et al., 2023). Common promoters

for iron CO₂-FT catalysts include potassium (K) (Qin et al., 2023), sodium (Na) (Ni et al., 2023), and manganese (Mn) (Singh et al., 2023). Incorporating cobalt into the iron catalyst can significantly alter surface properties, such as morphology, electronic structure, and chemical composition (Jiang et al., 2021). These modifications enhance CO₂ conversion efficiency and product selectivity by optimizing interactions between the catalyst and reactants. Cobalt can also influence reaction selectivity (Fan et al., 2021a), and adjusting the cobalt-to-iron ratio and other catalyst parameters allows for tailoring the selectivity towards specific hydrocarbons, such as long-chain alkanes, olefins, and oxygenates (Tsakoumis et al., 2010). In the RWGS reaction, adding cobalt can affect product distribution, favoring the formation of gases like methane or higher hydrocarbons (Díez-Ramírez et al., 2017; Fan et al., 2021b; Jiang et al., 2021).

Promoters in these catalysts function as either electronic or structural enhancers or both (Liu et al., 2021; Cele et al., 2019). Structural promoters help shape and stabilize the catalyst's active phase, leading to a more uniform dispersion on the support, which increases conversion rates. Electronic promoters modify local electron density near the catalyst's active site by donating or withdrawing electron density, influencing conversion levels and product selectivity (Ni et al., 2023; Sholeha et al., 2023). For instance, potassium acts as an electronic promoter in FT synthesis, enhancing CO₂ conversion and reducing methane yield while increasing the alkene/alkane ratio and promoting longer-chain hydrocarbons (Liu et al., 2021; Wang et al., 2023). Manganese serves a dual role as both a structural and electronic promoter for iron catalysts. When added to an iron catalyst, manganese suppresses methane formation and enhances the alkene/alkane ratio in both FT and CO₂ hydrogenation, functioning effectively as both a structural and electronic promoter (Kostyniuk et al., 2020; Jiang et al., 2021).

This study builds on current advancements by modifying a Fe-ZSM-5 catalyst with cobalt and incorporating potassium and manganese as promoters. The primary goal was to develop a more efficient catalyst for CO₂ hydrogenation to olefins. The catalyst comprised 4% cobalt and 4% iron, with 0.5% promoter concentrations. The performance of the synthesized catalysts was evaluated in a fixed-bed reactor and characterized using various techniques, including PXRD, FTIR, Pyridine-FTIR, XRF, N₂ adsorption, SEM, TEM, and EDS coupled with SEM.

2 Experimental

2.1 Materials

Zeolite Socony Mobil-5 with a SiO₂/Al₂O₃ ratio of 50, Iron (III) nitrate nonahydrate, Cobalt (II) nitrate hexahydrate, Manganese (II) nitrate hydrate and Potassium nitrate were all obtained from Sigma Aldrich. All the materials were used without further purification.

2.2 Ion exchange (IE) synthesis method

The Fe-ZSM-5 zeolites were synthesized by treating 1 g calcined ZSM-5 with Fe(NO₃)₃ salt in 20 mL deionized water, at 80°C for 3 h,

facilitating the exchange of H⁺ ions with iron. The resulting material was then calcined at 550°C for 6 h. For the preparation of cobalt-modified Fe-ZSM-5 (Co-Fe-ZSM-5), Fe(NO₃)₃ was replaced with Co(NO₃)₂ powder. Manganese and potassium promoters were introduced using the same ion exchange technique with Mn(NO₃)₂ and KNO₃, respectively.

2.3 Characterization

The chemical characteristics of surface functional groups in the zeolite catalysts were analyzed using FTIR spectra obtained across the vibrational range of 400 cm⁻¹–4,000 cm⁻¹ at room temperature. The measurements were taken using a Perkin Elmer Infrared spectroscope with a powder catalyst sample. The data were recorded and stored using Perkin Elmer software version 10.03.07. Pyridine-FTIR was done using the same instrument. Pyridine adsorption was performed at 200°C for 30 min, followed by evacuation at the same temperature for another 30 min to remove physisorbed pyridine.

Phase analysis was performed using a D8-Advance X-ray diffractometer from Bruker, operating in continuous θ - θ scan mode with Cu-K α radiation. The sample was positioned on a glass slide at the correct height. Measurements covered a 2θ range from 0.5° to 130° with a step size of 0.034°. Diffraction data were collected using a Lyn-Eye position-sensitive detector.

The morphology of the ZSM-5 catalysts was examined using a Hitachi HF-2000 TEM operating at 200 kV and a JEOL 6400F SEM. EDS analysis was incorporated into the SEM for atomic-level composition analysis. The morphology of the ZSM-5 catalysts was examined using a Hitachi HF-2000 TEM operating at 200 kV and a JEOL 6400F SEM. EDS analysis was incorporated into the SEM for atomic-level composition analysis. The morphology of the ZSM-5 catalysts was examined using a Hitachi HF-2000 TEM operating at 200 kV and a JEOL 6400F SEM. EDS analysis was incorporated into the SEM for atomic-level composition analysis.

The BET surface area, pore volume, and pore sizes of ZSM-5 were determined using a Microtrac 3300 Tristar Surface Area and Porosity Analyzer. Each sample, containing approximately 0.3 g of the material, underwent a degassing process before analysis. This involved heating the sample in the BET apparatus while flowing nitrogen (N₂) at 90°C for 1 hour, followed by further heating at 400°C for 4 hours. After preparation, the samples were loaded onto the analysis station, and the adsorbate was evaluated at a temperature of -195°C. The BET data was collected following an additional six-hour period.

XRF spectrometry was conducted using a PANalytical Axios Wavelength Dispersive spectrometer to determine major element compositions at the Central Analytical Facilities of Stellenbosch University in South Africa. This spectrometer, equipped with an Rh tube, utilized various analyzing crystals, including LIF200, LIF220, PE 002, Ge 111, and PX1. The instrument also featured a gas-flow proportional counter and a scintillation detector, employing a gas mixture of 90% Argon and 10% methane. Primary element analysis was carried out on fused glass disks utilizing a 2.4 kW Rhodium tube.

2.4 Catalyst testing

The zeolites were subjected to a compressive force of 30 bar, crushed, and then sieved to obtain particles sized between 2 and 3 mm. Exactly 1.000 g of the catalyst was loaded into a stainless-steel tube reactor, which was securely sealed at one end with quartz wool.

For catalyst preparation, an initial reduction step was conducted using a 10% H₂/N₂ gas mixture, flowing at 50 mL/min under atmospheric pressure in a tube furnace. This reduction process lasted for 4 h at 450°C. Following the reduction, the reactor was gradually cooled to 260°C. The CO₂ hydrogenation process was then carried out by introducing a high-pressure CO₂/H₂ gas mixture in a 1:4 ratio at a flow rate of 20 mL/min. This process occurred at 350°C under 20 bar pressure.

A Perkin Elmer Clarus 400 GC equipped with a 30 m × 530 μ m Suoelco Carboxen column and a thermal conductivity detector was utilized to analyze the CO₂ feed and CO product. Ethene, methanol, methane and pentene were analysed using a Shimadzu GC-2025 (Kyoto, Japan) with a Petro-Elite column (50 m length, 200 μ m diameter) and a flame ionization detector. The column temperature was initially maintained at 40°C for 5 min before being increased to 200°C at a rate of 3°C/min. All measurements were performed in triplicate.

After each performance test, the steel tube reactor was thoroughly cleaned. This involved multiple rinses with ethanol and deionized water to prevent cross-contamination. The reactor was then dried. Subsequently, the stainless-steel reactor, fitted with silica wool, underwent gas chromatography (GC) analysis after N₂ was introduced to confirm the removal of ethanol and any residual contaminants. CO₂ conversion was calculated using the formula:

$$CO_2 \text{ conversion (\%)} = \frac{CO_{2in} - CO_{2out}}{CO_{2in}} \times 100$$

where CO_{2in} and CO_{2out} were obtained from the amount of CO₂ at the inlet and outlet, respectively. The selectivity of the hydrocarbon products was calculated using the following equation:

$$C_nH_m \text{ selectivity (\%)} = \frac{n \times C_nH_m}{CO_{2in} - CO_{2out} - CO_{out}} \times 100$$

where C_nH_m represents the individual hydrocarbon product amounts in moles. The selectivity of CO was calculated according to the following equation:

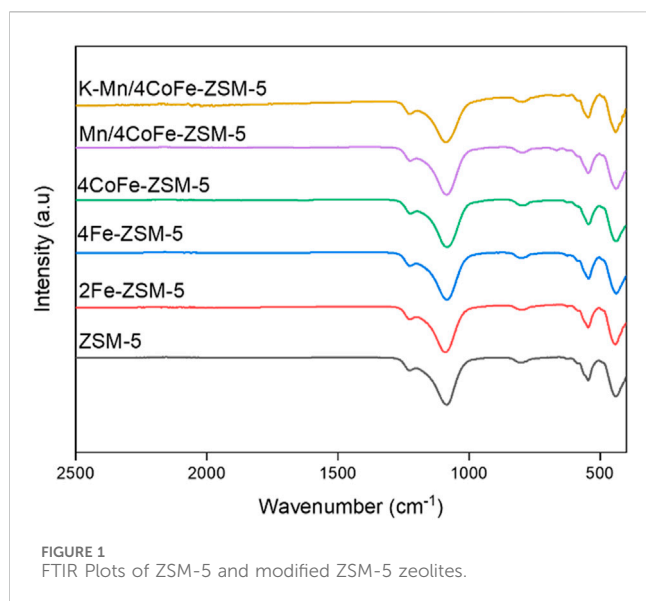
$$CO \text{ selectivity (\%)} = \frac{CO_{out}}{CO_{2in} - CO_{2out}} \times 100$$

where CO_{out} represents CO at the outlet amount.

3 Results and discussion

3.1 Structural and textural properties of catalysts

Figure 1 presents the FTIR spectra of the calcined catalysts in the 3900–400 cm⁻¹ range. Distinct absorption bands were observed at 1,087 cm⁻¹, 795 cm⁻¹, 547 cm⁻¹, and 441 cm⁻¹, corresponding to the asymmetric stretching vibrations characteristic of highly siliceous materials. The band at 441 cm⁻¹ is attributed to T-O-T (T = metal)



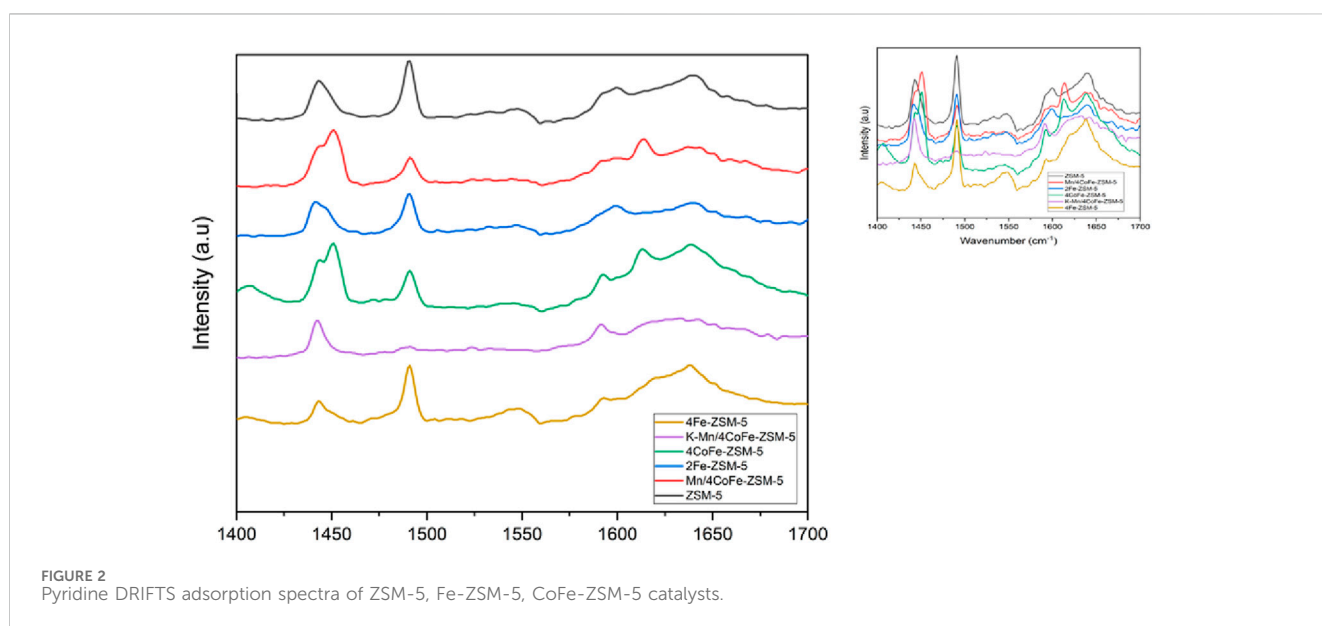
bending vibrations, while the 547 cm^{-1} band is linked to structure-sensitive vibrations from the double five-membered rings in the external linkage. During the ion exchange method, metal species occupy extra-framework positions within the ZSM-5 framework, which has a negative net charge. This occupation balances the zeolite charge, resulting in a stable interaction between the metal species and the zeolite structure. This interaction enhances the stability of the metal species and reduces their detachment and conglomeration. Additionally, absorption bands at $1,087$, 795 , and 441 cm^{-1} were associated with the symmetrical stretching of Si-O, asymmetrical stretching of Si-O, and the bending of Si-O/Al-O (SiO_4 and AlO_4 tetrahedron units), respectively. All samples displayed the primary characteristic vibrations of SiO_4 and AlO_4 , indicating that the zeolite structure remained intact after modification.

The acidity profiles of ZSM-5 and modified ZSM-5 catalysts were examined, and the resulting adsorption spectra are shown in Figure 2. As reported by Kostyniuk et al. (2020), bands corresponding to Bronsted acid sites (BAS) were identified at $1,545\text{ cm}^{-1}$, while Lewis acid sites (LAS) were indicated at $1,445\text{ cm}^{-1}$. The band at $1,489\text{ cm}^{-1}$ was attributed to pyridine adsorbed on both BAS and LAS, as well as H-bonded pyridine. Upon incorporating Fe species into ZSM-5 (2Fe-ZSM-5 and 4Fe-ZSM-5), the catalysts displayed a band at $1,445\text{ cm}^{-1}$ associated with Lewis-bonded pyridine. The presence of pyridine adsorption via hydrogen bonding at $1,489\text{ cm}^{-1}$ confirmed the existence of weak and medium Bronsted acid sites. Additionally, a band at $1,545\text{ cm}^{-1}$, linked to BAS, was also detected.

For the adsorption spectra of 4CoFe-ZSM-5. The catalyst displayed a band at $1,445\text{ cm}^{-1}$, corresponding to Lewis-bonded pyridine. In this Lewis region ($1,445\text{ cm}^{-1}$), a shift and peak splitting were observed compared to ZSM-5, consistent with observations by Dokania et al. (2020). This suggests the presence of multiple species with Lewis acidic character within the zeolite. A notable change of Bronsted acid sites (BAS) at $1,545\text{ cm}^{-1}$ was also observed. Peak splitting is observed with the introduction of Mn, indicated by a band at $1,624\text{ cm}^{-1}$ in the Mn/4CoFe-ZSM-5 catalyst, which was attributed to Lewis-bonded pyridine.

For K-Mn/4CoFe-ZSM-5, the Lewis acid sites (LAS) and Bronsted acid sites (BAS) were similar to those in the other catalysts, but they lacked the band at $1,489\text{ cm}^{-1}$, indicating a low presence of weak BAS. Due to the unique nature of the Lewis sites resulting from metal modification and the limited data on extinction coefficients, quantification of the acid sites could not be performed.

As shown in Figure 2, adding metals to ZSM-5 resulted in a significant change in Bronsted acid sites. These results suggest that metal incorporation into the ZSM-5 extra framework influences the Lewis acid sites while the Bronsted acid sites are affected. The reduction in Bronsted acidity hinders hydrogen transfer



reactions, leading to increased production of light olefins and reduced production of longer-chain hydrocarbons.

X-ray diffraction analysis was utilized to validate the crystallinity of the material. Figure 3 illustrates the XRD peaks for ZSM-5 and the modified ZSM-5 catalysts. All samples exhibited sharp and intense diffraction peaks, indicative of high crystallinity. No crystallinity alteration was observed when metals were loaded onto the zeolite. All ZSM-5-based adsorbents displayed peaks at $2\theta = 7.9^\circ$, 8.9° , 23.0° , and 23.9° , corresponding to the (101), (020), (332), and (303) planes of the MFI structure of zeolite (JCPDS). The diffraction peaks of all modified ZSM-5 catalysts remained consistent with those of the parent ZSM-5 in the 7° – 65° range, indicating retention of the ZSM-5 structure after metal treatment.

Figure 4 illustrates the N_2 adsorption-desorption isotherm curve of Mn/4CoFe-ZSM-5. Additional details can be found in the Supplementary Material. All catalysts exhibit type IV isotherms, which are characteristic of porous adsorbents. H4 hysteresis loops are observed at high relative pressures, indicating the presence of hollow spheres consisting of ordered mesoporous silica walls. The trend suggests increased N_2 adsorption as pores become filled at high relative pressures ($0.45 < p/p_0 < 0.95$). The absorption of nitrogen at pressure ratios of $P/P_0 = 0.3$ and 0.9 is attributed to the presence of intra- and interparticle pores, respectively. Notably, as the amount of metal increased, the number of intraparticles changed while interparticle pores increased. These modifications led to alterations in the surface area, as observed in Table 1. The pore size distribution of the zeolites was determined using the Barrett Joyner Halenda (BJH) approach, as shown in Figure 5. The catalysts exhibited a concentrated pore size of 2.2 nm.

The BET surface area, external surface area (S_{micro}), micropore volume, and mesopore volume of ZSM-5 catalysts obtained from the N_2 adsorption/desorption isotherms are presented in Table 2. The introduction of Co, Fe, and metal promoters (Mn and K) into the structure of the ZSM-5. The micropore volume experiences a minor change as the metal loading increases, possibly due to metal deposition either on the surface or inside the micropores, indicating minimal volume change.

The ZSM-5 support displayed a BET surface area of $419 \text{ m}^2/\text{g}$, which changes slightly with each metal loading but within the reported surface area range of ZSM-5. The combination of iron (Fe) and cobalt (Co) appears to promote improved dispersion of the metals as the metal loadings increase. An increase in the amount of metals on the catalysts might lead to a change in the surface area due to the dispersion of metals on the catalyst surface, resulting in a more significant number of active sites accessible to the reactant's molecules for the reaction. The specific surface area of 4Fe-ZSM-5 is $394 \text{ m}^2/\text{g}$, as determined by the BET method. After modifying the catalyst with 4% cobalt, the BET surface area slightly changed to $412 \text{ m}^2/\text{g}$.

3.2 Morphology and elemental characterization

Figures 6A–E showcases scanning electron microscope (SEM) images of both untreated ZSM-5 catalysts and those treated with metals. In the SEM micrographs of ZSM-5

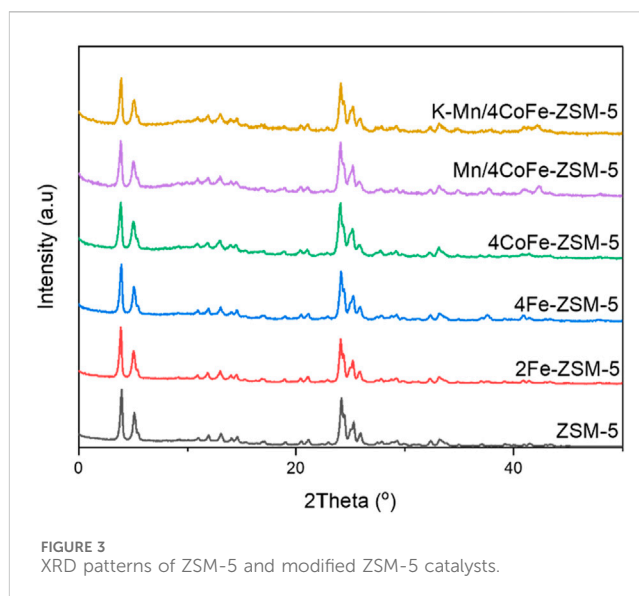


FIGURE 3 XRD patterns of ZSM-5 and modified ZSM-5 catalysts.

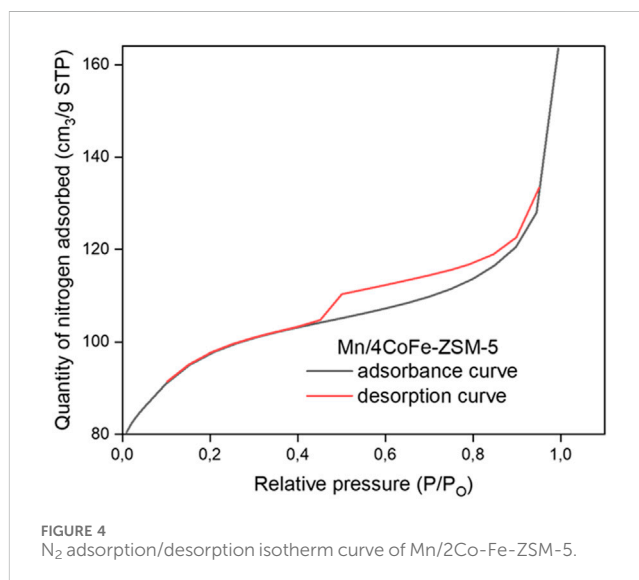


FIGURE 4 N_2 adsorption/desorption isotherm curve of Mn/2Co-Fe-ZSM-5.

zeolites (Figure 7A), the morphology of cuboids composed of aggregated crystal structures is observable. Notably, the absence of discernible textural alterations post-modification suggests that the ZSM-5 framework remained unchanged following the introduction of metals (Figures 7B–E). However, the morphology could benefit from improved resolution, predominantly consisting of condensed and clustered granular particles with a cubic and quasi-hexagonal form.

The particle size distribution was determined using the ImageJ program, revealing that all catalysts possess a mean particle size ranging from 101 to 150 nm, as indicated by the histograms in Figures 6A2–F2. Interestingly, the particle size distribution of the modified catalysts closely resembles that of the unmodified ZSM-5 catalysts after the introduction of metals. This particle size distribution across the modified catalysts indicates that differences in catalytic performance are likely influenced more by the nature of the promoters and their interactions with the CoFe-ZSM-5 framework.

TABLE 1 Textural properties of modified ZSM-5 catalysts.

Catalyst	SBET ^a (m ² /g)	S _{micro} ^b (m ² /g)	V _{meso} ^c (cm ³ /g)	V _{micro} ^b (cm ³ /g)
K-Mn/4Co-Fe-ZSM-5	343	298	0.87	0.12
Mn/4Co-Fe-ZSM-5	358	296	0.87	0.12
4CoFe-ZSM-5	412	305	0.87	0.12
4Fe-ZSM-5	394	341	0.85	0.14
2Fe-ZSM-5	407	302	0.86	0.12
ZSM-5	419	372	0.83	0.15

Mesopore surface area and volume were obtained by subtracting micropore area from the total.

^aBET method.

^bt-plot method.

^cV_{meso} = V_{ads} at p/p₀ = 0.99 - V_{micro}.

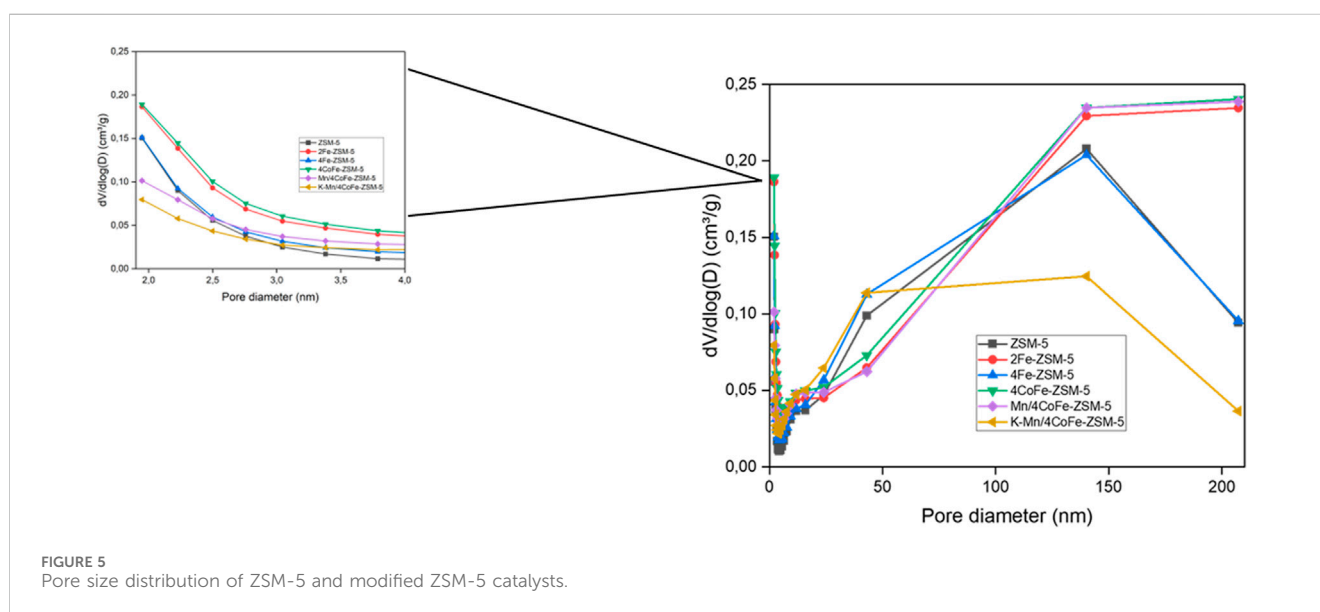


FIGURE 5 Pore size distribution of ZSM-5 and modified ZSM-5 catalysts.

TABLE 2 Elemental content from XRF analysis.

Catalyst	Al content (%)	Si content (%)	Fe content (%)	Co-content (%)	Mn content (%)	K Content (%)
K-Mn/4CoFe-ZSM-5	1.2	34.2	4.4	5.3	0.6	1.5
Mn/4CoFe-ZSM-5	1.2	34.8	4.7	7.7	0.6	0.0
4CoFe-ZSM-5	1.3	38.5	2.1	2.1	0.0	0.0
4Fe-ZSM-5	1.3	38.7	5.1	0.0	0.0	0.0
2Fe-ZSM-5	1.4	40.6	2.3	0.0	0.0	0.0
ZSM-5	1.4	41.7	0.0	0.0	0.0	0.0

Furthermore, a comprehensive elemental mapping study was conducted on the surface of ZSM-5 to unveil the distribution of Fe, Co, and Mn species (Supplementary Figures S12–S20). These images depict the spatial distribution of metals on a macroscopic level. Additionally, the TEM micrographs in Figures 6B1–F1 provide enhanced insight into the textural alterations. Ultimately, the remaining catalysts exhibited comparable properties, with relevant data accessible in the Supplementary Material.

Table 2 displays the quantities of aluminum (Al), silicon (Si), and other metals present in the modified ZSM-5. The table demonstrates the successful incorporation of metals into the ZSM-5 extra-framework. The XRF measurements reveal that more than 4% of Fe was incorporated into the zeolite 4Fe-ZSM-5. In addition, there was no noticeable decrease in the weight percentage of Fe for the Mn/4CoFe-ZSM-5 catalyst following modification. This was accomplished because of metal ions being

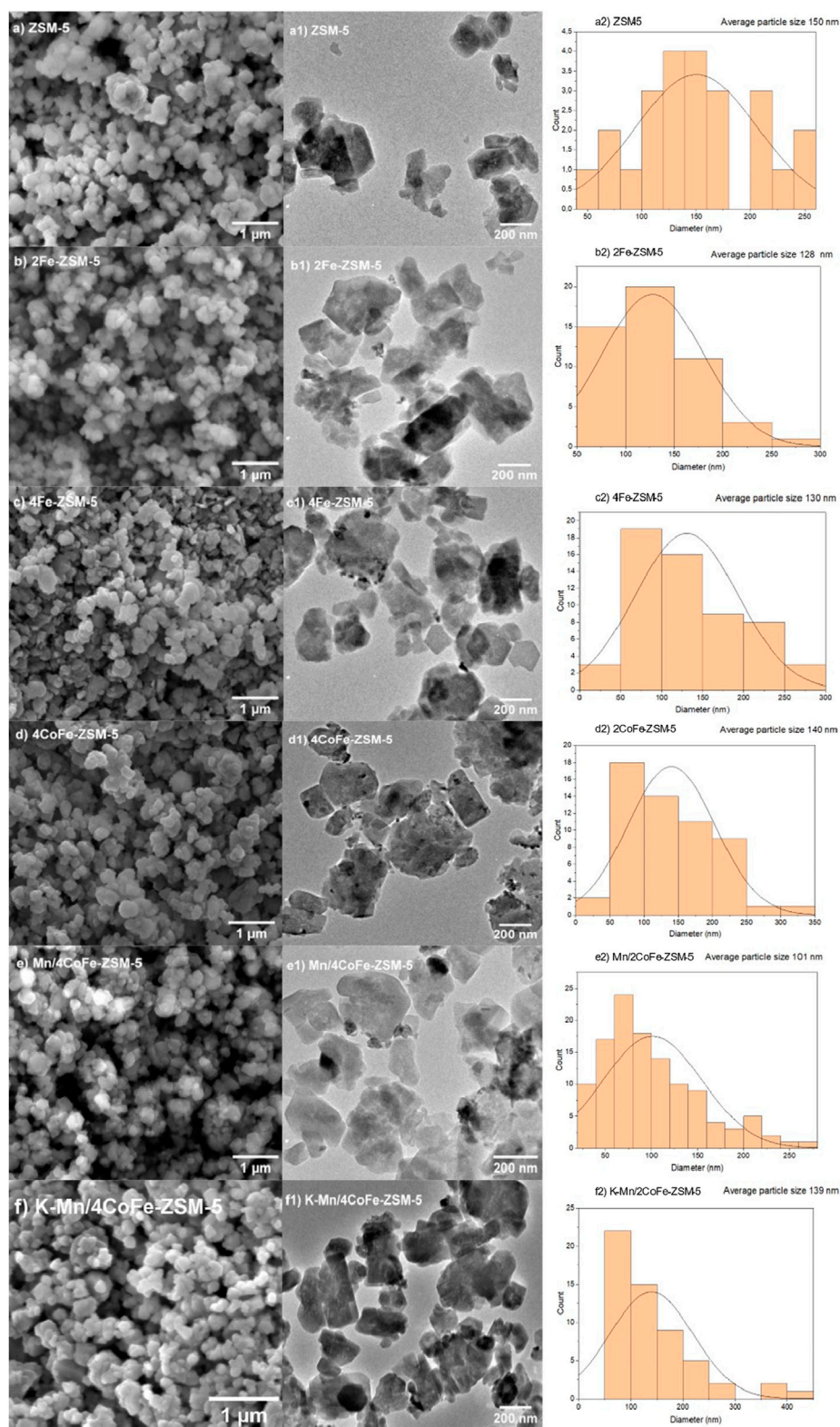


FIGURE 6
(A–F) SEM and TEM images of ZSM-5 and the modified catalysts, **(A1–F1)** histograms of particle size distributions of ZSM-5 and the modified catalysts **(A2–F2)**.

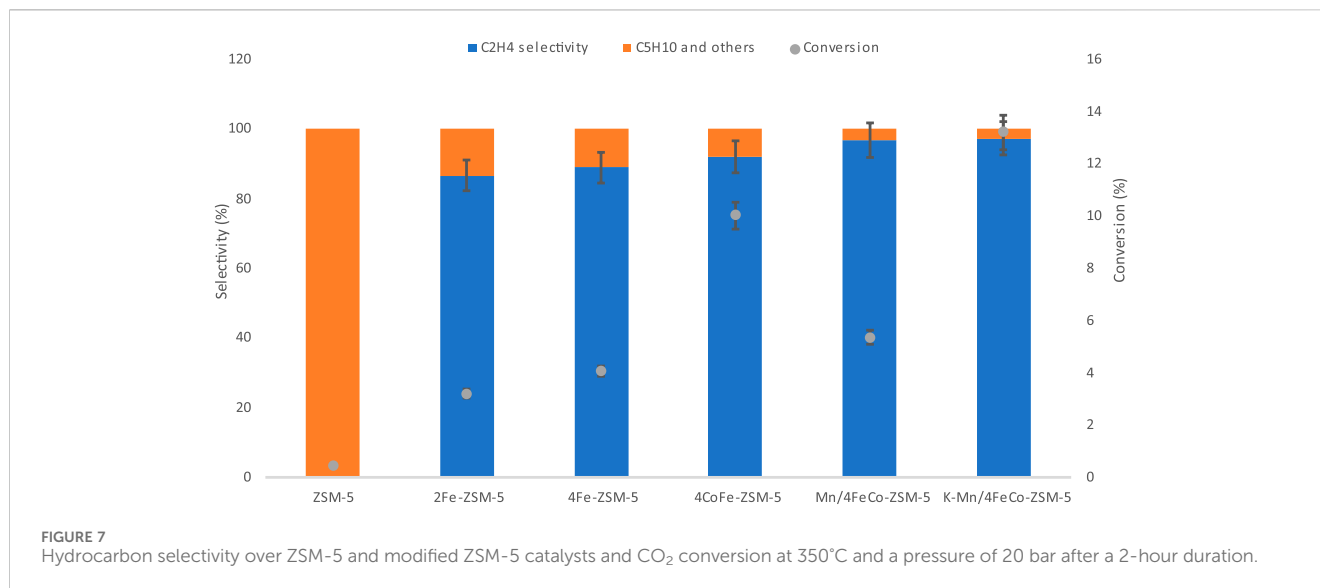


TABLE 3 Catalytic performance of ZSM-5 and modified ZSM-5 catalysts.

Catalyst	CO ₂ conversion percentage (%)	Product selectivity (%)		Hydrocarbon distribution (%)			
		CO	HC	CH ₃ OH	CH ₄	C ₂ H ₄	C ₅ H ₁₀
K-Mn/4Co-Fe-ZSM-5	13.2	1.5	98.5	0.2	0.1	97.3	0.9
Mn/4Co-Fe-ZSM-5	5.3	2.4	97.6	0.6	0.1	96.7	0.2
4Co-Fe-ZSM-5	10.1	7.5	92.4	0	0.4	92.1	0
4Fe-ZSM-5	4.1	0	100	9.4	1.5	88.9	0.2
2Fe-ZSM-5	3.2	0	100	11.5	1.7	86.7	0.1
ZSM-5	0.4	0	100	0	100	0	0

Reaction at 350°C, under 20 bar pressure with CO₂/H₂ gas mixture, in a 1:4 ratio, at a flow rate of 20 mL/min at duration of 2 h.

retained in the extra-framework when potassium is exchanged onto the zeolite extra-framework. A similar phenomenon is seen on K-Mn/4CoFe-ZSM-5. The K was accurately substituted into the catalyst, whereas the amount of Mn was below the anticipated level. The aluminium (Al) content remained consistent, whereas the silicon (Si) content declined. Among the samples, K-Mn/4CoFe-ZSM-5 had the lowest Si content. The decrease in silicon content enhances the acidity of the catalyst, resulting in a greater preference for olefins (Jiang et al., 2020).

3.3 Catalytic performance

The catalytic activity experiments were conducted under a CO₂ and H₂ mixture at a temperature of 350°C and a pressure of 20 bar, following a reduction step at 450°C. A concise summary of the collected data after a 2-h duration during the reaction is provided in Table 3 and Figures 7, 8. According to Table 3, a CO₂ conversion rate of 3.2% was observed with a 2 wt% Fe loading on the ZSM-5 support. The low CO₂ conversion over metal-modified ZSM-5 is primarily due to the low weight percentage of the active metals. The selectivity

of C₂H₄ (ethene) was measured to be 86.7%. Additionally, byproducts such as C₅H₁₀, CO, CH₄, and CH₃OH were also generated. Figure 7 and Table 3 illustrate that the catalyst with a deposition of 4 wt% Fe on ZSM-5 exhibited higher CO₂ conversion to ethene compared to the catalyst with 2%wt Fe. Specifically, the 4Fe ZSM-5 catalyst achieved a CO₂ conversion rate of 4.1% with a selectivity of 88.9% towards C₂H₄. Furthermore, the selectivity towards ethene was enhanced with higher weight percentages of Fe. It can be inferred that the conversion of CO₂ increased as the quantity of deposited Fe on the support increased. The reduction in surface area with increasing Fe content did not adversely impact ethene selectivity, suggesting that selectivity is determined more by the characteristics of the active sites than by the surface area. These results are consistent with previous studies where the increase in metal loading also resulted in higher CO₂ conversion and selectivity towards ethene, indicating that our proposed catalyst is competitive with those previously reported (Kostyniuk et al., 2020; Yuan et al., 2023a).

The enhanced hydrocarbon selectivity was attributed to the effective conversion of CO₂ into hydrocarbons, indicating that the active sites for Fischer-Tropsch synthesis of the Fe-ZSM-

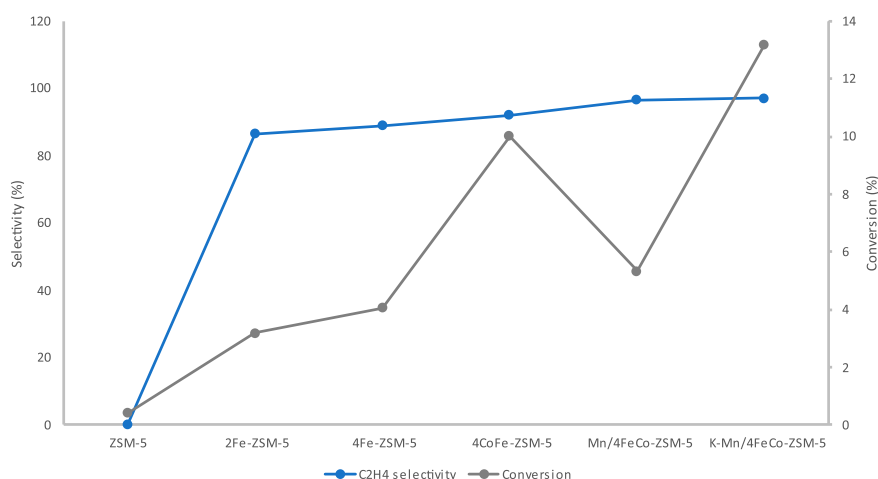


FIGURE 8
C₂H₄ selectivity over ZSM-5 and modified ZSM-5 catalysts and CO₂ conversion at 350°C and a pressure of 20 bar after a 2-hour duration.

5 catalysts exhibited high activity. The occurrence of the Reverse Water Gas Shift (RWGS) reaction was attributed to magnetite iron (Fe₃O₄) or amorphous oxide phase. In contrast, chain growth necessitated the presence of a carbide phase, primarily χ -Fe₅C₂ (Jiang et al., 2020). These findings align with reference (Dokania et al., 2020). The Fe-ZSM-5 catalyst primarily comprised the Fe₃O₄ phase, with small amounts of iron carbide, resulting in a reduced ability to produce long-chain hydrocarbons (C₅H₁₀). The Fe-ZSM-5 catalysts showed no selectivity to CO product.

Table 3 demonstrates a significant improvement in C₂H₄ selectivity and CO₂ conversion upon deposition of Co onto the Fe-ZSM-5 catalysts. The selectivity 4CoFe-ZSM-5 exhibited a selectivity of 92.1% to C₂H₄ with a CO₂ conversion rate of 10.1%. The notable improvement in CO₂ conversion and C₂H₄ selectivity arises from the 1:1 Fe to Co weight percentage ratio (Table 2), which is crucial for maximizing CO₂ conversion efficiency and light olefin selectivity (Yang et al., 2017; Hua et al., 2023). This is attributed to the complementary catalytic functions and synergistic interaction between iron and cobalt. An enhanced CO selectivity is recorded, indicating the heightened reactivities of the RWGS reaction because of the presence of cobalt. Fe-Co contact during the hydrogenation reaction over the CoFe-ZSM-5 catalysts facilitated the creation of Co-Fe carbide, Co₂C, and θ -Fe₃C phases. This mechanism prevented the excessive hydrogenation of both CO and CH₃OH intermediates into methane and light olefins into alkanes. The presence of both metallic and acidic functions on metal carbides is advantageous for the process of CO₂ hydrogenation due to the easy absorption of CO₂ in carbides. The addition of Co showed 7.5% selectivity to CO product.

An improvement in C₂H₄ selectivity of 96.7% was seen when the catalysts were modified with Mn. A decline in CH₄ selectivity (0.08%) and CO₂ conversion (5.3%) is observed. The decrease in hydrocarbon (HC) selectivity occurred because the addition of manganese (Mn) to iron (Fe) catalysts reduces the formation of methane (CH₄) while enhancing the production of olefins. The addition of trace amounts of Mn can greatly enhance the activity of the catalyst (Chen et al., 2024). XRF analysis, as shown in Table 2,

verified that the Mn/4Co-Fe-ZSM-5 catalyst contained 0.6 weight percent of manganese. Additionally, the decrease in CO₂ conversion is accompanied by the increase in selectivity to C₂H₄. It is observed that the addition of Mn to 4CoFeZSM-5 reduced the CO selectivity from 7.5% to 2.4%.

Once again the surface area (Table 1) did not adversely impact the selectivity as the addition of K to the catalyst led to a substantial increase in CO₂ conversion while the selectivity to C₂H₄ was still significantly high, even though the surface area decreased. The rise is attributed to the promotion of CO₂ conversion facilitated by the addition of alkaline substances. In the Fischer-Tropsch process, excessive K deactivates the iron catalyst, making it essential to use only minimal amounts (Dorner et al., 2010). As confirmed by XRF small amounts of K were exchanged onto the catalyst. The addition of K to the catalyst considerably enhanced the selectivity of C₂H₄. The improvement in selectivity was a result of the promotion of K, which caused a notable shift in the production of olefins. The exceptional catalytic performance (13.2% CO₂ conversion, 97.3% C₂H₄ selectivity) seen in the presence of potassium (K) can be attributed to the enhanced ability of CO₂ chemisorption and the inhibition of H₂ adsorption. The potassium also assisted in reducing the CO selectivity further as 1.5% selectivity to CO was obtained. This, in turn, improves the likelihood of C-C bond formation. Ethene (C₂H₄) was the predominant product obtained with all of the catalysts. This could be attributed to the limited re-adsorption of C₂ products on the catalyst surface, which hindered the formation of C₃-C₅ products by chain growth. The rate of CO₂ hydrogenation in unmodified ZSM-5 zeolite compared to metal-modified ZSM-5 zeolite can differ significantly due to the influence of metal species on the catalytic activity and reaction pathways. In its unmodified form, ZSM-5 zeolite exhibits very small intrinsic catalytic activity towards CO₂ hydrogenation, primarily driven by its acidic sites and pore structure. However, the catalytic activity is limited compared to metal-modified counterparts (Yuan et al., 2023b). This is shown on Table 3. The activity evaluation was performed with triplicate measurements, yielding 97.3% ± 0.9% at a 95% confidence level. This highlights the precision of the measurements and the reproducibility of the results.

The increased selectivity to pentene, can be attributed to the catalytic properties of the K modified catalyst, which favors the production of long chain olefins. The incorporation of metals such as Fe, Co, K, and Mn likely alters the acid site distribution and balances hydrogenation and dehydrogenation steps, suppressing the formation of other hydrocarbons while enhancing pentene selectivity (Wang et al., 2024).

Metal modification significantly alters the activity of the CO₂ hydrogenation reaction. The presence of metal species can enhance the adsorption of reactants and intermediates, thereby increasing the likelihood of reaction occurrence and improving the reaction rate at the reaction conditions. Different metals exhibited varying selectivities towards specific products, such as methanol, ethene and pentene (Table 3). Faster reaction kinetics would be expected over the metal modified ZSM-5 due to enhanced catalytic activity and increased availability of active sites provided by the metal species. Metal-modified ZSM-5 may require regeneration steps to maintain catalytic activity, as metal species can undergo deactivation through processes such as sintering or poisoning (Zhao, 2010). However, metal ions introduced via ion exchange are typically held on the zeolite structure through strong electrostatic interactions with the negatively charged framework. This stabilization might minimize the migration and agglomeration of metal species during thermal treatment, thereby reducing the likelihood of sintering (Urquieta-González et al., 2002; Li et al., 2022). Furthermore, the extra framework is accessible to the substrate and the products are not highly confined and are able to undergo desorption after the reaction.

Chen et al. (2024) conducted a study on the effects of manganese and zinc promoters on ferrite catalysts for CO₂ hydrogenation. The reaction was carried out at 300°C, with a gas mixture ratio of CO₂: H₂ = 1:3 at a flow rate of 10 mL min⁻¹ and a total pressure of 6 bar. They found that Mn additives led to a CO₂ conversion of 11% and a selectivity towards C₂₊ hydrocarbons of 5%. (Yuan et al., 2023a). attempted to boost the production of light Olefins from CO₂ Hydrogenation over Fe–Co bimetallic catalysts. They did this under the following conditions: 320°C, p = 3 MPa, gas hourly space velocity (GHSV) = 7,200 mL.gcat⁻¹ h⁻¹, and H₂/CO₂/N₂ = 63/21. Their best catalyst FeCo-9:1 exhibited a selectivity of C₂₊ olefins over 36% and a CO₂ conversion higher than 40%. In this study we investigated the effect of Co, Fe, and Mn on the activity of ZSM-5 in CO₂ hydrogenation. The CO₂ hydrogenation process was carried out at temperature of 350°C and a pressure of 20 bar, introducing a high-pressure CO₂/H₂ gas mixture, in a 1:4 ratio, at a flow rate of 20 mL/min. The catalyst with the best activity was K-Mn/4Co-Fe-ZSM-5 with a CO₂ conversion of 13% and 97% selectivity to C₂H₄.

4 Conclusion

In this investigation, Co, Mn, and K were successfully introduced into the extra-framework of Fe-based ZSM-5 zeolite. Various analytical techniques were employed to examine structural and morphological changes, including FTIR, pyridine FTIR, XRD, SEM, TEM, EDS, and XRF. The FTIR studies indicated a shift towards shorter wavelengths when metals were added, confirming

the presence of Co, Fe, Mn, and K species. Pyridine FTIR revealed altered acidic sites, with a peak splitting indicating increased Lewis acidity post-metal modification. XRD diffractograms affirmed the retention of zeolite crystallinity, with characteristic MFI structures observed. BET analysis showed microporous characteristics, while the SEM and TEM images illustrated spherical shapes and confirmed uniform metal distribution. The catalytic performance results demonstrate that metal modifications significantly enhance both CO₂ conversion and olefin (C₂H₄) selectivity, with potassium-modified Mn/4Co-Fe-ZSM-5 achieving the highest conversion (13.2%) and selectivity (97.3%). The improved activity is attributed to the synergistic effects of metal species on active site formation and reaction pathways, particularly through promoting olefin production and minimizing methane formation. These findings underscore the potential of tailored metal modifications to optimize ZSM-5 catalysts for sustainable olefin production, offering a competitive edge in CO₂ Hydrogenation techniques. The results show that Mn and K improved the selectivity of olefins by reducing the selectivity to CO on the Co-Fe-ZSM-5 catalyst.

Data availability statement

The original contributions presented in the study are included in the article/[Supplementary Material](#), further inquiries can be directed to the corresponding author.

Author contributions

PM: Formal Analysis, Investigation, Methodology, Writing–original draft. MC: Conceptualization, Funding acquisition, Investigation, Methodology, Resources, Supervision, Validation, Writing–review and editing. MM: Methodology, Resources, Supervision, Writing–review and editing.

Funding

The author(s) declare that financial support was received for the research, authorship, and/or publication of this article. This research was funded by the National Research Foundation, the Sasol foundation and the Northwest University Postgraduate bursary.

Acknowledgments

The technical staff at NWU (Murendeni Ravele and Sizwe Loyilani) and Neo Sehloko.

Conflict of interest

The authors declare that the research was conducted in the absence of any commercial or financial relationships that could be construed as a potential conflict of interest.

Generative AI statement

The author(s) declare that no Generative AI was used in the creation of this manuscript.

Publisher's note

All claims expressed in this article are solely those of the authors and do not necessarily represent those of their affiliated organizations, or

References

- Abanades, J. C., Rubin, E. S., Mazzotti, M., and Herzog, H. J. (2017). On the climate change mitigation potential of CO₂ conversion to fuels. *Energy Environ. Sci.* 10 (12), 2491–2499. doi:10.1039/c7ee02819a
- Al-Shafei, E. N., Aljishi, A. N., Shakoor, Z. M., Albahar, M. Z., Aljishi, M. F., and Alasseel, A. (2023). Steam catalytic cracking and lump kinetics of naphtha to light olefins over nanocrystalline ZSM-5 zeolite. *RSC Adv.* 13 (37), 25804–25816. doi:10.1039/d3ra03157h
- Cele, M., Friedrich, H., and Bala, M. (2019). Evaluation of silanization of Na-Fe-silicalite-1 and Na-Fe-ZSM-5 on the oxidation of n-octane to C₈ oxygenates. *Journal of Porous Materials* 26 (5). doi:10.1007/s10934-019-00731-z
- Cele, M. N. (2014). Activation of n-octane and cyclohexane to oxygenates using modified zeolites.
- Chen, C. J., Oh, J., Yang, A. C., Zhou, C., Liccardo, G., Sapru, S., et al. (2024). Understanding the effects of manganese and zinc promoters on ferrite catalysts for CO₂ hydrogenation to hydrocarbons through colloidal nanocrystals. *Surf. Sci.* 741, 122424. doi:10.1016/j.susc.2023.122424
- Chen, J., Han, S. J., Park, H. G., Nasriddinov, K., Zhang, C., Jun, K. W., et al. (2023). Benchmarking promoters of Fe/activated carbon catalyst for stable hydrogenation of CO₂ to liquid hydrocarbons. *Appl. Catal. B Environ.* 325, 122370. doi:10.1016/j.apcatb.2023.122370
- Díez-Ramírez, J., Sánchez, P., Kyriakou, V., Zafeiratos, S., Marnellos, G. E., Konsolakis, M., et al. (2017). Effect of support nature on the cobalt-catalyzed CO₂ hydrogenation. *J. CO₂ Util.* 21, 562–571. doi:10.1016/j.jcou.2017.08.019
- Dokania, A., Dutta Chowdhury, A., Ramirez, A., Telalovic, S., Abou-Hamad, E., Gevers, L., et al. (2020). Acidity modification of ZSM-5 for enhanced production of light olefins from CO₂. *J. Catal.* 381, 347–354. doi:10.1016/j.jcat.2019.11.015
- Dorner, R. W., Hardy, D. R., Williams, F. W., and Willauer, H. D. (2010). K and Mn doped iron-based CO₂ hydrogenation catalysts: detection of KAlH₄ as part of the catalyst's active phase. *Appl. Catal. A General* 373 (1–2), 112–121. doi:10.1016/j.apcata.2009.11.005
- Edelmannová, M., Lin, K.-Y., Wu, J. C. S., Troppová, I., Čapek, L., and Kočí, K. (2018). Photocatalytic hydrogenation and reduction of CO₂ over CuO/TiO₂ photocatalysts. *Appl. Surf. Sci.* 454, 313–318. doi:10.1016/j.apsusc.2018.05.123
- Errero, J. L. (2023). Impact of loadshedding in South Africa: a CGE analysis. *J. Econ. Political Econ.*, 78–94.
- Fan, J., Wu, H., Liu, R., Meng, L., Fang, Z., Liu, F., et al. (2021a). Non-thermal plasma combined with zeolites to remove ammonia nitrogen from wastewater. *J. Hazard. Mater.* 401, 123627. doi:10.1016/j.jhazmat.2020.123627
- Fan, T., Liu, H., Shao, S., Gong, Y., Li, G., and Tang, Z. (2021b). Cobalt catalysts enable selective hydrogenation of CO₂ toward diverse products: recent progress and perspective. *J. Phys. Chem. Lett.* 12 (43), 10486–10496. doi:10.1021/acs.jpcllett.1c03043
- Fedorov, A., Lund, H., Kondratenko, V. A., Kondratenko, E. V., and Linke, D. (2023). Elucidating reaction pathways occurring in CO₂ hydrogenation over Fe-based catalysts. *Appl. Catal. B Environ.* 328, 122505. doi:10.1016/j.apcatb.2023.122505
- Gao, J., Choo Sze Shiong, S., and Liu, Y. (2023). Reduction of CO₂ to chemicals and fuels: thermocatalysis versus electrocatalysis. *Chem. Eng. J.* 472, 145033. doi:10.1016/j.cej.2023.145033
- García-Hurtado, E., Rodríguez-Fernández, A., Moliner, M., Martínez, C., and Technology (2020). CO₂ hydrogenation using bifunctional catalysts based on K-promoted iron oxide and zeolite: influence of the zeolite structure and crystal size. *Catal. Sci. Technol.* 10 (16), 5648–5658. doi:10.1039/d0cy00712a
- Guo, L., Gao, X., Gao, W., Wu, H., Wang, X., Sun, S., et al. (2022). High-yield production of liquid fuels in CO₂ hydrogenation on a zeolite-free Fe-based catalyst. *Chem. Sci.* 14 (1), 171–178. doi:10.1039/d2sc05047a
- Hua, Z., Yang, Y., and Liu, J. (2023). Direct hydrogenation of carbon dioxide to value-added aromatics. *Coord. Chem. Rev.* 478, 214982. doi:10.1016/j.ccr.2022.214982
- Jiang, F., Wang, S., Zheng, J., Liu, B., Xu, Y., and Liu, X. (2021). Fischer-Tropsch synthesis to lower α -olefins over cobalt-based catalysts: dependence of the promotional effect of promoter on supports. *Catal. Today* 369, 158–166. doi:10.1016/j.cattod.2020.03.051
- Jiang, J., Rong, B. G., and Feng, X. (2023). Olefin production via methanol integrated with light hydrocarbon conversion: novel process designs, techno-economic analysis, and environmental analysis. *Industrial Eng. Chem. Res.* 62 (37), 15036–15050. doi:10.1021/acs.iecr.3c01319
- Jiang, J., Wen, C., Tian, Z., Wang, Y., Zhai, Y., Chen, L., et al. (2020). Manganese-Promoted Fe₃O₄ microsphere for efficient conversion of CO₂ to light olefins. *Industrial and Eng. Chem. Res.* 59 (5), 2155–2162. doi:10.1021/acs.iecr.9b05342
- Kostyniuk, A., Key, D., and Mdeleeni, M. (2020). 1-hexene isomerization over bimetallic M-Mo-ZSM-5 (M: Fe, Co, Ni) zeolite catalysts: effects of transition metals addition on the catalytic performance. *J. Energy Inst.* 93 (2), 552–564. doi:10.1016/j.joei.2019.06.009
- Li, Y., Yellezuome, D., Li, C., and Liu, R. (2022). Deactivation mechanism and regeneration effect of bi-metallic Fe-Ni/ZSM-5 catalyst during biomass catalytic pyrolysis. *Fuel* 312, 122924. doi:10.1016/j.fuel.2021.122924
- Li, Y., Zeng, L., Pang, G., Wei, X., Wang, M., Cheng, K., et al. (2023). Direct conversion of carbon dioxide into liquid fuels and chemicals by coupling green hydrogen at high temperature. *Appl. Catal. B Environ.* 324, 122299. doi:10.1016/j.apcatb.2022.122299
- Li, Z., Wang, J., Qu, Y., Liu, H., Tang, C., Miao, S., et al. (2017). Highly selective conversion of carbon dioxide to lower olefins. *ACS Catal.* 7 (12), 8544–8548. doi:10.1021/acscatal.7b03251
- Liang, J., Guo, L., Gao, W., Wang, C., Guo, X., et al. (2022). Direct conversion of CO₂ to aromatics over K-Zn-Fe/ZSM-5 catalysts via a fischer-tropsch synthesis pathway. *Industrial Eng. Chem. Res.* 61 (29), 10336–10346. doi:10.1021/acs.iecr.1c05061
- Liu, R., Leshchev, D., Stavitski, E., Juneau, M., Agwara, J. N., and Porosoff, M. D. (2021). Selective hydrogenation of CO₂ and CO over potassium promoted Co/ZSM-5. *Appl. Catal. B Environ.* 284, 119787. doi:10.1016/j.apcatb.2020.119787
- Liu, W., Cheng, S., Malhi, H. S., Gao, X., Zhang, Z., and Tu, W. (2022). Hydrogenation of CO₂ to olefins over iron-based catalysts: a review. *Catalysts* 12 (11), 1432. doi:10.3390/catal12111432
- Luo, W., Li, B., Xu, M., Pang, C., Lester, E., and Kow, K. W. (2023). Accelerated curing of cement mortar: in-situ carbonation utilising CO₂-impregnated faujasite. *Constr. Build. Mater.* 388, 131639. doi:10.1016/j.conbuildmat.2023.131639
- Muñoz, I., and Weidema, B. P. (2024). Ethylene and propylene production from steam cracking in Europe: a consequential perspective. *Int. J. Life Cycle Assess.* 29, 745–758. doi:10.1007/s11367-024-02282-1
- Ni, Z., Cai, M., Zhong, S., Chen, X., Shen, H., and Su, L. (2023). Sodium promoted FeZn@SiO₂-C catalysts for sustainable production of low olefins by CO₂ hydrogenation. *Catalysts* 13 (12), 1508. doi:10.3390/catal13121508
- Ojelade, O. A., and Zaman, S. F. (2021). A review on CO₂ hydrogenation to lower olefins: understanding the structure-property relationships in heterogeneous catalytic systems. *J. CO₂ Util.* 47, 101506. doi:10.1016/j.jcou.2021.101506
- Ou, H., Ning, S., Zhu, P., Chen, S., Han, A., Kang, Q., et al. (2022). Carbon nitride photocatalysts with integrated oxidation and reduction atomic active centers for improved CO₂ conversion. *Angew. Chem. - Int. Ed.* 61, e202206579. doi:10.1002/anie.202206579
- Qin, C., Du, Y., Wu, K., Xu, Y., Li, R., Fan, H., et al. (2023). Facet-Controlled Cu-doped and K-promoted Fe₂O₃ nanosheets for efficient CO₂ hydrogenation to liquid hydrocarbons. *Chem. Eng. J.* 467, 143403. doi:10.1016/j.cej.2023.143403
- Raje, A., Inga, J. R., and Davis, B. H. (1997). Fischer-Tropsch synthesis: process considerations based on performance of iron-based catalysts. *Fuel* 76 (3), 273–280. doi:10.1016/s0016-2361(96)00185-8

those of the publisher, the editors and the reviewers. Any product that may be evaluated in this article, or claim that may be made by its manufacturer, is not guaranteed or endorsed by the publisher.

Supplementary material

The Supplementary Material for this article can be found online at: <https://www.frontiersin.org/articles/10.3389/fchem.2025.1562436/full#supplementary-material>

- Ronda-Lloret, M., Rothenberg, G., and Shiju, N. R. (2019). A critical look at direct catalytic hydrogenation of carbon dioxide to olefins. *ChemSusChem* 12 (17), 3896–3914. doi:10.1002/cssc.201900915
- Saeidi, S., Amin, N. A. S., and Rahimpour, M. R. (2014). Hydrogenation of CO₂ to value-added products—a review and potential future developments. *J. CO₂ Util.* 5, 66–81. doi:10.1016/j.jcou.2013.12.005
- Satthawong, R., Koizumi, N., Song, C., and Prasassarakich, P. (2015). Light olefin synthesis from CO₂ hydrogenation over K-promoted Fe–Co bimetallic catalysts. *Catal. Today* 251, 34–40. doi:10.1016/j.cattod.2015.01.011
- Sholeha, N. A., Holilah, H., Bahruji, H., Ayub, A., Widiastuti, N., Ediati, R., et al. (2023). Recent trend of metal promoter role for CO₂ hydrogenation to C1 and C2+ products. *South Afr. J. Chem. Eng.* 44, 14–30. doi:10.1016/j.sajce.2023.01.002
- Singh, G., Khurana, D., Khan, T. S., Ghosh, I. K., Chowdhury, B., Khodakov, A. Y., et al. (2023). Insight into Mn enhanced short-chain olefins selectivity in CO₂ hydrogenation over Na–CuFeO₂ catalyst. *Appl. Surf. Sci.* 616, 156401. doi:10.1016/j.apsusc.2023.156401
- Sun, S., Zhang, C., Wang, Y., Zhao, X., Sun, H., and Wu, C. (2023). CO₂ capture from H₂O and O₂ containing flue gas integrating with dry reforming methane using Ni-doping CaO dual functional materials. *Chem. Eng. J.* 468, 143712. doi:10.1016/j.cej.2023.143712
- Tang, J., Mayyas, M., Ghasemian, M. B., Sun, J., Rahim, M. A., et al. (2022). Liquid-metal-enabled mechanical-energy-induced CO₂ conversion. *Adv. Mater.* 34 (1), e2105789. doi:10.1002/adma.202105789
- Tsakoumis, N. E., Rønning, M., Borg, Ø., Rytter, E., and Holmen, A. (2010). Deactivation of cobalt based Fischer–Tropsch catalysts: a review. *a Rev.* 154 (3–4), 162–182. doi:10.1016/j.cattod.2010.02.077
- Urquieta-González, E., Martins, L., Peguin, R., and Batista, M. (2002). Identification of extra-framework species on Fe/ZSM-5 and Cu/ZSM-5 catalysts typical microporous molecular sieves with zeolitic structure. *Mat. Res.* 5, 321–327. doi:10.1590/s1516-14392002000300017
- Visconti, C. G., Martinelli, M., Falbo, L., Fratolocchi, L., and Lietti, L. (2016). CO₂ hydrogenation to hydrocarbons over Co and Fe-based Fischer–Tropsch catalysts. *Catal. Today* 277, 161–170. doi:10.1016/j.cattod.2016.04.010
- Wang, K., Li, Z., Gao, X., Ma, Q., Zhang, J., Zhao, T.-S., et al. (2024). Novel heterogeneous Fe-based catalysts for carbon dioxide hydrogenation to long chain α -olefins—A review. *Environ. Res.* 242, 117715. doi:10.1016/j.envres.2023.117715
- Wang, L., Han, Y., Wei, J., Ge, Q., Lu, S., Mao, Y., et al. (2023). Dynamic confinement catalysis in Fe-based CO₂ hydrogenation to light olefins. *Appl. Catal. B Environ.* 328, 122506. doi:10.1016/j.apcatb.2023.122506
- Wang, Z., and Zhang, Z. (2023). Interfacial catalysis of metal-oxide nanocatalysts in CO₂ hydrogenation to value-added C1 chemicals. *Surf. Sci. Technol.* 1 (1), 9. doi:10.1007/s44251-023-00009-2
- Weber, D., Gandotra, A., Schossig, J., Zhang, H., Wildy, M., Wei, W., et al. (2023). Promoter effect on carbon nanosphere-encapsulated Fe–Co catalysts for converting CO₂ to light olefins. *Catalysts* 13 (11), 1416. doi:10.3390/catal13111416
- Weber, J. L., del Monte, D. M., Beerthuis, R., Dufour, J., Martos, C., de Jong, K. P., et al. (2021). Conversion of synthesis gas to aromatics at medium temperature with a Fischer–Tropsch and ZSM-5 dual catalyst bed. *Catalysis Today* 369, 175–183.
- Wei, J., Yao, R., Han, Y., Ge, Q., and Sun, J. (2021). Towards the development of the emerging process of CO₂ heterogeneous hydrogenation into high-value unsaturated heavy hydrocarbons. *Chem. Soc. Rev.* 50 (19), 10764–10805. doi:10.1039/d1cs00260k
- Wen, C., Li, T., Huang, Z., and Kang, Q. K. (2023). Oxidative dehydrogenation of alkanes through homogeneous base metal catalysis. *Chem. Rec.* 23 (11), e202300146. doi:10.1002/tcr.202300146
- Xu, Y., Zhai, P., Deng, Y., Xie, J., Liu, X., Wang, S., et al. (2020). Highly selective olefin production from CO₂ hydrogenation on iron catalysts: a subtle synergy between manganese and sodium additives. *Angew. Chem. - Int. Ed.* 59 (48), 21736–21744. doi:10.1002/anie.202009620
- Yang, H., Dang, Y., Cui, X., Bu, X., Li, J., Li, S., et al. (2023). Selective synthesis of olefins via CO₂ hydrogenation over transition-metal-doped iron-based catalysts. *Appl. Catal. B Environ.* 321, 122050. doi:10.1016/j.apcatb.2022.122050
- Yang, H., Zhang, C., Gao, P., Wang, H., Li, X., Zhong, L., et al. (2017). A review of the catalytic hydrogenation of carbon dioxide into value-added hydrocarbons. *Catal. Sci. Technol.* 7, 4580–4598. doi:10.1039/C7CY01403A
- Yuan, F., Zhang, G., Wang, M., Zhu, J., Zhang, M., Ding, F., et al. (2023a). Boosting the production of light olefins from CO₂ hydrogenation over Fe–Co bimetallic catalysts derived from layered double hydroxide. *Industrial Eng. Chem. Res.* 62 (21), 8210–8221. doi:10.1021/acs.iecr.3c00439
- Yuan, F., Zhang, G., Wang, M., Zhu, J., Zhang, M., Ding, F., et al. (2023b). Boosting the production of light olefins from CO₂ hydrogenation over Fe–Co bimetallic catalysts derived from layered double hydroxide. *Industrial Eng. Chem. Res.* 62 (21), 8210–8221. doi:10.1021/acs.iecr.3c00439
- Zhao, X. (2010). “Porous materials for direct and indirect evaporative cooling in buildings,” in *Materials for energy efficiency and thermal comfort in buildings* (Elsevier), 399–426.
- Zhou, J., Liu, M., Bai, S., Sun, J., Wei, J., and Wang, J. (2024). Well-dispersed MOF-5 on the polyvinylpyrrolidone-coated random lamellas of clinoptilolites for adsorptive separation performance of CO₂, CH₄, and N₂. *Adv. Sustain. Syst.* 8, 2300466. doi:10.1002/adsu.202300466